Fast passive microwave radiative transfer in precipitating clouds: Towards direct radiance assimliation

Ralf Bennartz *, Thomas Greenwald, Chris O'Dell
University of Wisconsin-Madison

Andrew Heidinger
NOAA/NESDIS

1. Introduction

Passive microwave measurements from space have perhaps the greatest potential for improving global weather analyses because they offer 3D temperature and humidity information in both clear and cloudy conditions and provide information on cloud water mass and 3D precipitation structure. Indeed, assimilation of microwave-derived rainfall and moisture satellite products has shown to significantly improve short-range weather forecasts and the quality of global analyses of moisture and vertical motion (Hou et al. 2001). But direct assimilation of microwave radiance data offers benefits over products derived from radiances. For example, radiance assimilation is not subject to biases from initial guesses and a priori assumptions as are product retrievals, and it allows for better control of background errors in the assimilation environment. As a first step in radiance assimilation in all-weather conditions, observed and global model-produced microwave radiances have been compared in order to evaluate the ability of these models to produce clouds and precipitation (Chevallier and Bauer 2003; Chevallier et al. 2001).

This study, which is supported by the newly formed Joint Center for Satellite Data Assimilation (JCSDA), seeks to develop and test fast radiative transfer modeling systems in preparation for direct assimilation of microwave radiance satellite data (current and future) into NCEP's Global Data Analysis System (GDAS) under all weather conditions, especially precipitating clouds. GDAS currently uses a 3DVAR approach to assimilate SSM/I surface wind speed and precipitation products and radiance data from the Advanced Microwave Sounding Unit (AMSU) but in clear-sky only (Derber and Wu 1998; McNally et al. 2000). Our main goal, therefore, is to extend the capability of GDAS to include microwave radiance data in cloudy and precipitating systems over the oceans. This means incorporating multiple scattering radiative transfer (RT) models since precipitation-size particles scatter microwave radiation primarily at the higher frequencies. Here we give preliminary results of RT calculations at AMSU frequencies using coarser resolution version of the NCEP Global Forecast System (GFS) model output but focusing on clear and nonprecipitating cloudy areas. More complete results for precipitating clouds will be presented at the symposium.

2. Data

2.1 *Global model*

The current version of NCEP's GFS uses a spectral atmospheric model with horizontal resolution at T254 (about 0.5 x 0.5 deg. latitude/longitude) and 64 vertical levels in sigma coordinates. The deep convection scheme is based on Pan and Wu (1994), while shallow convection is parameterized following Tiedtke (1983). The percent area of cloud coverage for a given grid point is not predicted but computed from the relative humidity, saturation specific humidity (q) and a minimum threshold of q using the approach of Xu and Randall (1996). Cloud water and ice are both predicted via a scheme by Zhao and Carr (1997).

GFS degraded products (1^o x 1^o horizontal grid and 26 vertical levels) were used in the analysis since they were readily available online at ftp://ftpprd.ncep. noaa.gov/pub/data/nccf/com/avn/prod. The 12 hr forecast products were selected for the following quantities: temperature, relative humidity, and cloud

Corresponding author address: Ralf Bennartz, Atmospheric and Oceanic Sciences, University of Wisconsin – Madison, 1225 W. Dayton St., Madison, WI, USA, e-mail: Bennartz@aos.wisc.edu

liquid water mixing ratio at all levels; surface temperature, 10 m wind vector, and precipitation rate at the ground. Neither cloud ice mixing ratio nor instantaneous cloud fraction was available.

2.2 *Satellite*

NOAA's AMSU-A/B instrument suite is designed mainly to observe global temperature and humidity at different layers in the atmosphere but it also provides important information on water clouds and precipitation (summarized in Tables 1 and 2). AMSU scans across the direction of motion of the satellite, extending to about $\pm 48^o$ from nadir. It currently flies on the NOAA-15, -16, and -17 satellites.

We utilized the 1^o x 1^o gridded AMSU brightness temperature products available from the NOAA/NESDIS ftp site that are produced separately for each of the three satellites and the ascending and descending nodes. To provide independently determined cloud coverage for the microwave data, AVHRR cloud amount products were obtained using the NOAA operational cloud detection algorithm. These data were also transferred to a 1^o x 1^o grid.

Table 1. AMSU-A characteristics.

Chan	Frequency (GHz)	Sensitivity
1	23.8	Boundary layer (BL) water vapor, surface, precipitation
2	31.4	Water clouds, surface, BL water vapor, precipitation
3	50.3	BL temp, water clouds, precipitation
4	52.8	Lower troposphere temp
5	53.596±0.115	Mid-troposphere temp
6	54.4	Upper troposphere temp
7	54.94	Upper troposphere temp
8	55.50	Lower stratosphere temp
9	f_o=57.290344	Lower stratosphere temp
10	f_o±0.217	Mid-stratosphere temp
11	f_o±0.3222±0.048	Upper stratosphere temp
12	f_o±0.3222±0.022	Upper stratosphere temp
13	f_o±0.3222±0.010	Upper stratosphere/lower mesosphere temp
14	f_o±0.3222±0.0045	Mesosphere temp
15	89.0	BL water vapor, water clouds, surface, precipitation

Table 2. AMSU-B characteristics.

Chan	Frequency (GHz)	Sensitivity
16	89.0±0.9	BL water vapor, water clouds, surface, precipitation
17	150.0±0.9	BL water vapor, water clouds, surface, precipitation
18	183.31±1.00	Upper troposphere water vapor
19	183.31±3.00	Mid-troposphere water vapor
20	183.31±7.00	Lower troposphere water vapor

3. Radiative Transfer Modeling

The RT model tested here to compute brightness temperatures for a given set of model atmospheric and surface parameters is an Eddington two-stream method for plane-parallel conditions (Bauer 2002). The method also incorporates delta scaling to improve accuracy when particles become large compared to incident wavelength (forward scattering becomes greater), such as encountered with large precipitation particles. These methods are accurate to within about 1-2 K under a wide range of conditions when compared to more exact methods (Smith et al. 2002).

Required as input to the two-stream RT model are the effective single-scattering properties of the medium (i.e., extinction, single-scatter albedo, and asymmetry factor) and boundary conditions (i.e., ocean surface emissivity and skin temperature). Single-scattering properties for rain, snow, graupel and hail

were computed from Mie theory at discrete frequencies, temperatures and water contents, assuming an exponential size distribution and ice densities. These calculations were organized in tabular form for interpolation purposes. Because the GFS data products included precipitation rate at the surface only, several crude assumptions were made to vertically distribute the total rate into liquid and ice species. A constant rain rate was assumed from the surface up to cloud base. From there, the fraction of ice (liquid water) precipitation rates was linearly increased (decreased) from 0 to 1 (1 to 0) until a temperature of –20^{o} C was reached, above which only ice existed. Cloud liquid water and ice were similarly partitioned from the freezing level to –20^{o} C. Precipitation rates were converted to water content using an exponential size distribution. Extinction coefficients for gas (water vapor and oxygen) were obtained from OPTRAN (McMillin et al. 1995), which is the gas absorption model used operationally by GDAS, while absorption due to cloud liquid water was computed from Liebe et al. (1992).

As discussed by Chevallier and Bauer (2003), both cloud fraction (which varies vertically) and how clouds are distributed vertically in the volume that comprises a grid point in the model have an impact on computed brightness temperatures. Unfortunately, modeled cloud amount was not available to us, so it was assumed that clouds were completely overcast. Cloud overlap was also not considered. These issues will be addressed in future work.

Finally, ocean surface emissivity was computed from FASTEM-2, a model originally developed by English and Hewison (1998) and further refined and improved by Deblonde and English (2000). The main input variables that FASTEM-2 requires are surface skin temperature, observation zenith angle, frequency, and wind speed at 10 m height.

4. Results

As a consistency check, we first compared clear sky brightness temperatures computed at selected frequencies from the Eddington two-stream model against the existing absorption-only RT model currently in the operational GDAS. Figure 1 shows the 89-GHz brightness temperature field calculated from the two-stream model. Differences between the RT model results were found to be less than 0.1 K (see Fig. 2). However, at one of the frequencies that corresponds to the humidity sounding channel on AMSU-B (channel 18), differences as large as -0.85 K were seen (Fig. 3). It was discovered that these differences were related to the treatment of the thermal source within the model layer. The absorption-only RT model assumes a layer average temperature within the layer, while in the Eddington two-stream model, temperature was allowed to vary linearly throughout the layer. Differences between the RT models are drastically diminished to under –0.0007 K when both use the same thermal source treatment (not shown). Ordinarily this is not an issue if the model vertical grid spacing is sufficiently small. Apparently, the grid spacing is too coarse in the upper troposphere where this channel's weighting function peaks. Use of full resolution GFS data should significantly reduce such differences, however.

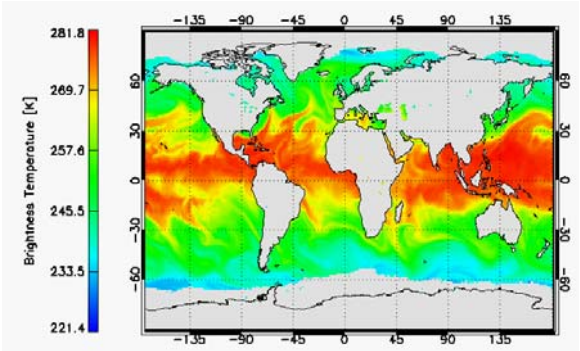

Figure 1: 89 GHz brightness temperature field computed at nadir for clear sky from GFS model output (15 October, 2003 12 hr forecast starting at 06Z) using the Eddington two-stream radiative transfer model.

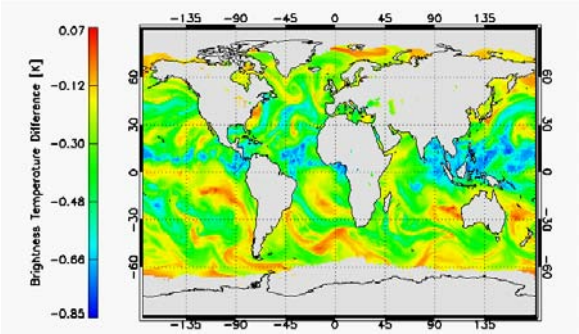

Figure 2: Differences between clear sky 89 GHz brightness temperatures computed from the Eddington model and NCEP's operational absorption-only radiative transfer model for same time as Fig. 1.

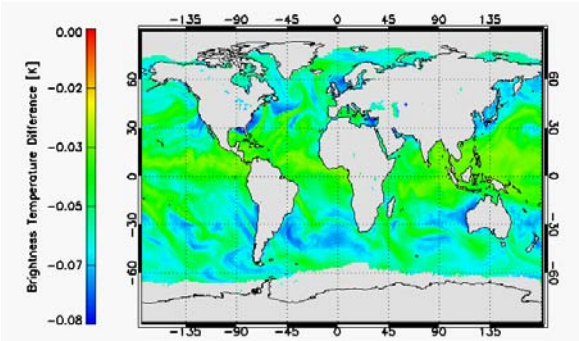

Figure 3: Same as Figure 2 but for AMSU-B channel 18 frequency at a zenith angle of 53°.

Comparisons between simulated and observed brightness temperatures were performed over 4 days (16-19 Oct. 2003) using a time difference of less than 1 hr for the AMSU-A/B window channels (1, 2, 16 and 17) and AMSU-B humidity sounding channels (18-20). Cloud-free regions were defined from the AVHRR-derived products as less than 5% cloudiness, whereas cloudy regions were considered greater than 95% cloudiness.

A qualitative comparison between AVHRR-derived cloud cover, AMSU-B 89 GHz brightness temperature field, and simulated brightness temperature field is given for one time period in Figures 4, 5, and 6 respectively. Outside of convectively active regions of precipitation, many spatial features in the simulated brightness temperature field correspond well with the observed field.

Quantitative comparisons over the 4-day time period for strictly cloud-free regions revealed biases at some frequencies (Fig. 7). Similar biases existed for all three satellites indicating the biases are likely not caused by calibration errors. The large differences at 89 GHz and 150 GHz may be related to uncertainties in characterizing the gaseous absorption, which is more uncertain in spectral window regions; although it may also be due to biases in the GFS model predictions of boundary layer humidity or the surface emissivity model. The noticeable zenith angle dependent bias suggests either a problem with the gas optical path for larger angles or angular deficiencies in the microwave surface emissivity model.

For cloudy nonprecipitating cases, biases are overall smaller and the angle dependent biases are not as prominent although they still remain at the lower frequency channels (Fig. 8). These results suggest that, in general, the GFS model predictions of cloud water mass are reasonable, at least during this time period.

A first calculation of the brightness temperatures at 150 GHz including precipitation is shown in Figure 9. In regions of convective precipitation, scattering by large ice particles plays the major role in causing large depressions in the brightness temperatures at this frequency. Depressions of 30-40 K relative to the background (cloud liquid + gas) are common.

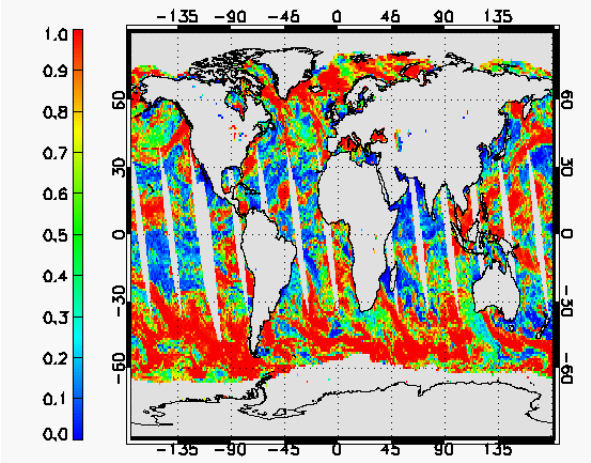

Figure 4: Cloud fraction determined from the NOAA-16 AVHRR for ascending overpasses on 16 October 2003.

5. Conclusions

Preliminary test results of a RT forward modeling system for computing microwave radiances from GSF model parameters compared against AMSU observations has been very encouraging. The system consists of an Eddington two-stream RT model, OPTRAN, FASTEM-2 surface emissivity model, and lookup tables for precipitation scattering properties. Comparisons with NCEP's operational absorption-only RT model under clear skies shows excellent agreement, especially at AMSU water vapor sounding channels. Limited comparisons between brightness temperatures computed from GFS 12 hr forecast fields and AMSU measurements under clear sky conditions showed zenith angle dependent biases for the window frequencies, while comparisons under cloudy cases had the best agreement.

We are currently developing an RT model based on successive orders of scattering; results of which may be presented at the symposium as well.

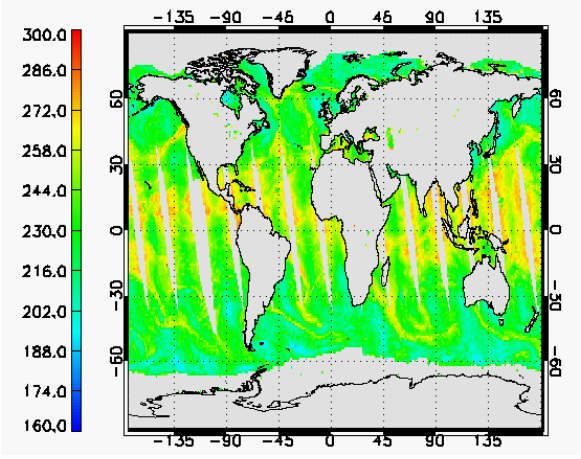

Figure 5: Gridded AMSU-B 150 GHz (channel 17) brightness temperature product for same day as Fig. 4.

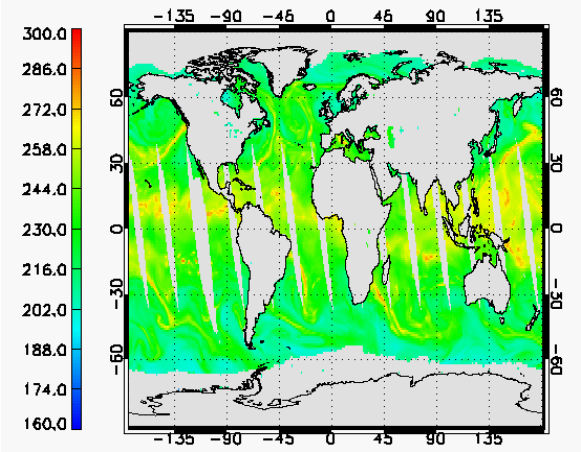

Figure 6: Simulated AMSU-B channel 17 brightness temperatures at nadir conditions and excluding precipitation for 12 hr forecast beginning at 00Z on 16 October 2003.

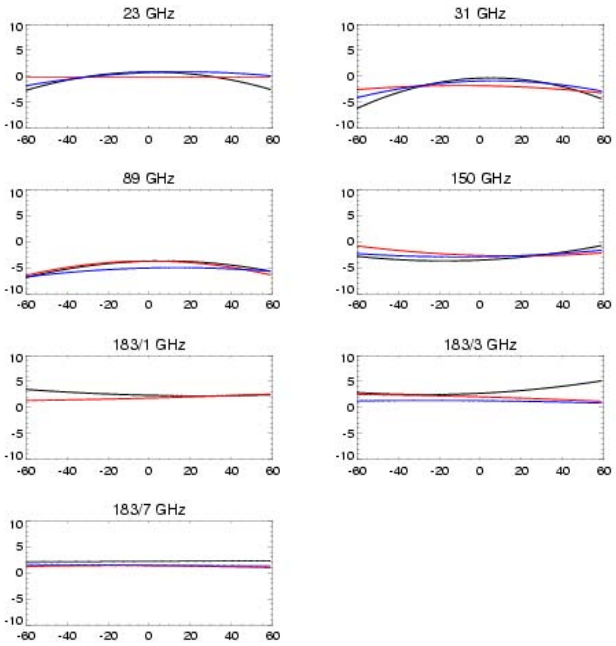

Figure 7: Observed minus simulated brightness temperatures as a function of zenith angle for selected AMSU-A/B channel frequencies under clear sky conditions. Black lines are for NOAA-15, red for NOAA-16, and blue for NOAA-17.

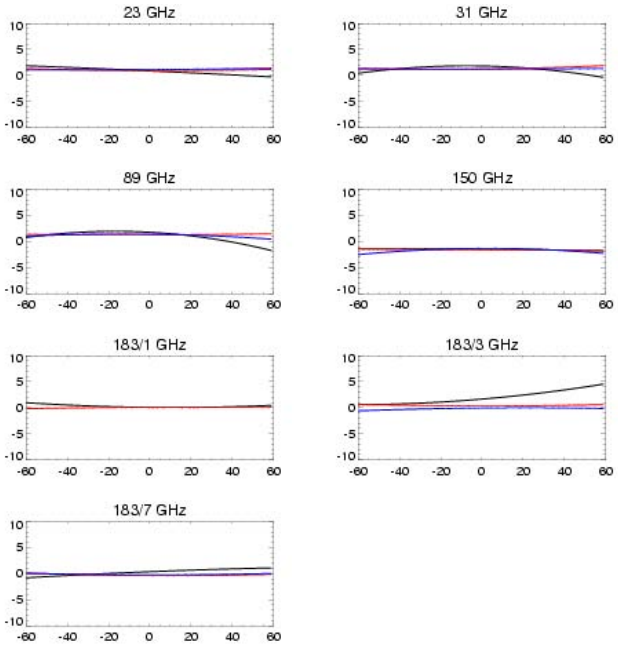

Figure 8: Same as Figure 7 but for cloudy cases.

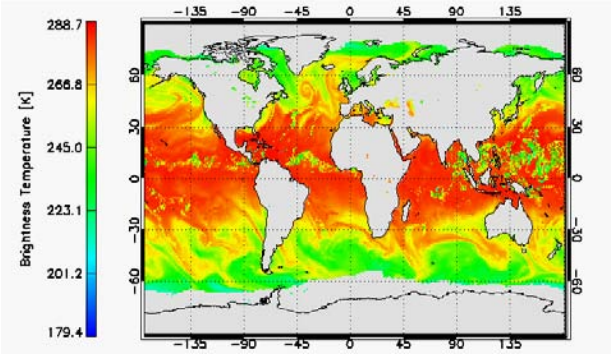

Figure 9: Simulated 150 GHz brightness temperature field that includes precipitation for 15 October, 2003 and 12 hr forecast beginning at 06Z.

6. Acknowledgements

Support was provided by a JCSDA grant through NOAA cooperative agreement NA07EC0676. Thanks go to the UK Met office for use of RTTOV-7. Also greatly appreciated are the contributions of our colleagues, Peter Bauer at ECMWF and Ken Campana at NOAA/NCEP.

7. References

Bauer, P., 2002: Microwave radiative transfer modeling in clouds and precipitation. Part I: Model description. NWP SAF Rep. NWPSAF-EC-TR-006, 27 pp.

Chevallier, F. and P. Bauer, 2003: Model rain and clouds over oceans: Comparison with SSM/I observations, *Mon. Wea. Rev*., **131**, 1240-1255.

Chevallier, F., P. Bauer, G. Kelly, C. Jakob, and T. McNally, 2001: Model clouds over oceans as seen from space: Comparison with HIRS/2 and MSU radiances. *J. Climate*, **14**, 4216-4229.

Deblonde, G., and S. J. English, 2000: Evaluation of the FASTEM-2 microwave oceanic surface emissivity model. *Proc. Int. TOVS Study Conf*., Budapest, Hungary, ITWG/IAMAS, 67-78.

Derber, J. C., and W.-S. Wu, 1998: The use of TOVS cloud-cleared radiances in the NCEP SSI analysis system. *Mon. Wea. Rev*., **126**, 2287-2299.

English, S., and T. J. Hewison, 1998: A fast generic millimetre wave emissivity model. *Proc. SPIE*, 3503, 22-30.

Hou, A. Y., S. Q. Zhang, A. M. da Silva, W. S. Olson, C. D. Kummerow, and J. Simpson, 2001: Improving global analysis and short-range forecast using rainfall and moisture observations derived from TRMM and SSM/I passive microwave sensors. *Bull. Amer. Meteor. Soc*., **82**, 659-679.

Liebe, H. J., P. Rosenkranz, and G. A. Hufford, 1992: Atmospheric 60 GHz oxygen spectrum: New laboratory measurements and line parameters. *J. Quant. Spectros. Radiat. Transfer*, **48**, 629-643.

McNally, A. P., J. C. Derber, W.-S. Wu and B. B. Katz, 2000: The use of TOVS level-1B radiances in the NCEP SSI analysis system. *Quart. J. Roy. Meteor. Soc*., **126**, 689-724.

McMillin, L. M., L. J. Crone, M. D. Goldberg, and T. J. Kleespies, 1995. Atmospheric transmittance of an absorbing gas, 4. OPTRAN: A computationally fast and accurate transmittance model for absorbing gases with fixed and variable mixing ratios at variable viewing angles, *Appl. Opt*., 34, 6269-6274.

Pan, H.-L., and W.-S. Wu, 1995: Implementing a mass flux convection parameterization package for the NMC medium-range forecast model. NMC Office Note, No. 409, 40 pp. [Available from NCEP, 5200 Auth Road, Washington, DC 20233]

Smith, E. A., and others, 2002: Intercomparison of microwave radiative transfer models for precipitating clouds, *IEEE Trans. on Geosc. and Remote Sens.* **40**, 541-549.

Tiedtke, M., 1983: The sensitivity of the time-mean large-scale flow to cumulus convection in the ECMWF model. ECMWF Workshop on Convection in Large-Scale Models, 28 November-1 December 1983, Reading, England, pp. 297-316.

Xu, K. M., and D. A. Randall, 1996: A semiempirical cloudiness parameterization for use in climate models. *J. Atmos. Sci*., **53**, 3084-3102.

Zhao, Q. Y., and F. H. Carr, 1997: A prognostic scheme for operational NWP models. *Mon. Wea. Rev*., **125**, 1931-1953.

Proceedings of the Thirteenth International TOVS Study Conference

INTERNATIONAL ATOVS WORKING GROUP

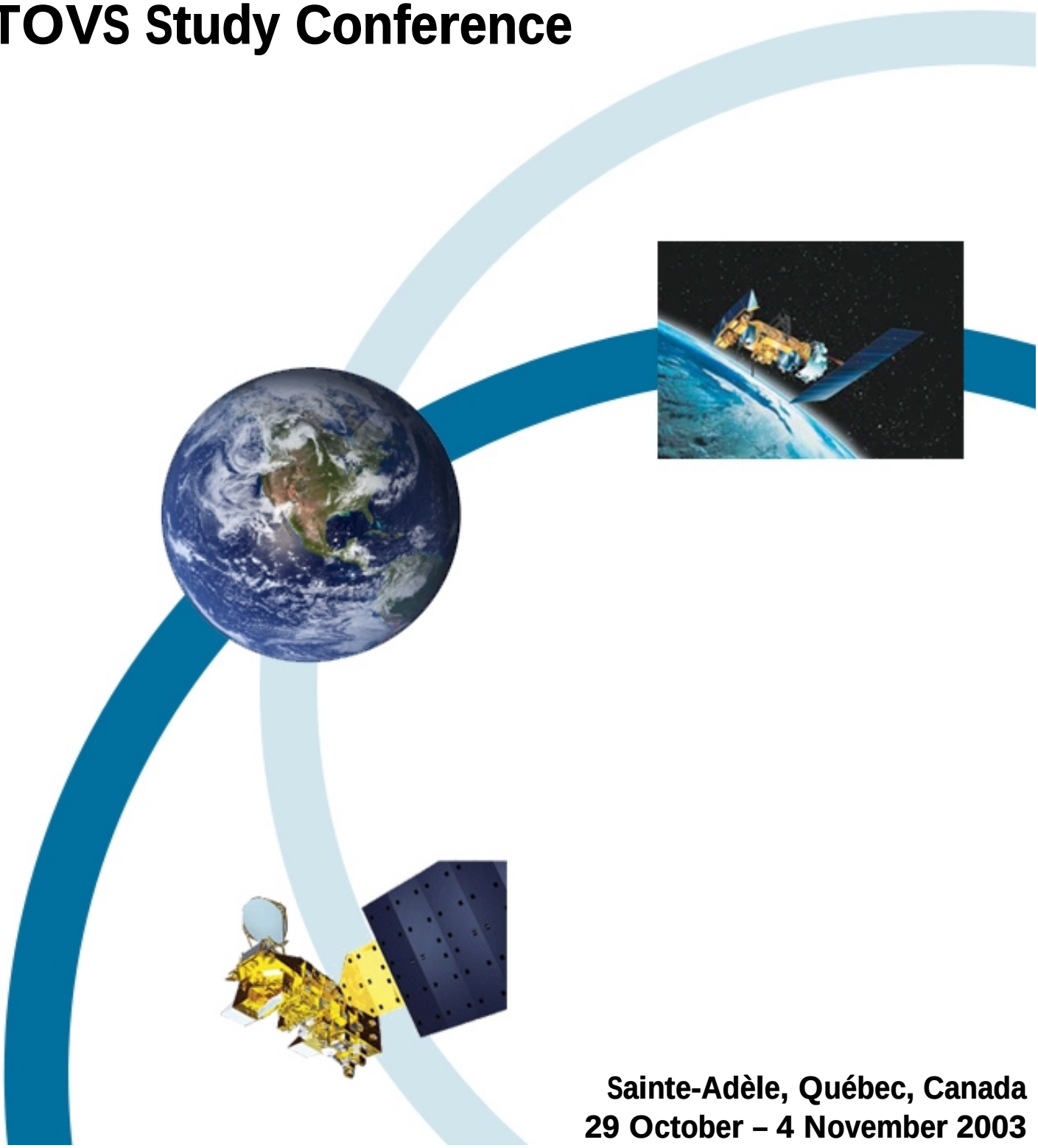

Sainte-Adèle, Québec, Canada
29 October – 4 November 2003